

Representation of Turbulent Mixing and Buoyancy Reversal in Bulk Cloud Models

WOJCIECH W. GRABOWSKI

Mesoscale and Microscale Meteorology Division, National Center for Atmospheric Research, Boulder, Colorado*

(Manuscript received 18 September 2006, in final form 30 January 2007)

ABSTRACT

This paper discusses the representation of subgrid-scale turbulent mixing in bulk models of warm (ice free) clouds, which assume instantaneous adjustment to grid-scale saturation. This is a reasonable assumption for condensation of water vapor because supersaturations inside clouds are typically small ($\sim 0.1\%$ or smaller), except near cloud bases where about an order of magnitude larger supersaturations are anticipated. For the cloud evaporation, however, instantaneous adjustment to grid-scale saturation is questionable, especially when evaporation occurs as a result of turbulent mixing between a cloud and its unsaturated environment. This is because turbulent mixing between initially separated volumes of cloudy and cloud-free environmental air proceeds through a gradual filamentation of these volumes, with progressively increasing evaporation of cloud water during the approach to final homogenization. A relatively simple model of this chain of events is included in a bulk model of moist nonprecipitating thermodynamics. The model delays adjustment to saturation for cloud evaporation following the turbulent mixing until the volume can be assumed homogeneous. An additional prognostic variable, the width of a cloudy filament, is added to represent the progress of turbulent mixing and the approach to homogenization. Theoretical developments are illustrated by idealized 2D simulations of moist thermals rising from rest and realistic large-eddy simulations of a cloud field.

1. Introduction

Bulk approach is commonly used in modeling of warm (i.e., ice free) clouds to represent the effects of condensation and evaporation. In this approach, the amount of water vapor that condenses or evaporates is equal to the amount required to maintain exact saturation over the model grid box. Since the actual supersaturations (with respect to water saturation) that occur inside ice-free clouds are usually small (a few tenths of a percent or less), the bulk assumption is reasonably accurate as far as the condensation is concerned (cf., Kogan and Martin 1994 and references therein). When evaporation of cloud water is considered—especially in the context of a turbulent mixing between a cloud and its unsaturated environment (e.g., Austin et al. 1985;

Paluch and Baumgardner 1989; Malinowski and Zawadzki 1993)—such an approach may be inappropriate because undersaturations occurring during evaporation of cloud water are not necessarily small. Typically, turbulent mixing between cloudy and cloud-free air results in a significant delay of the homogenization over model-resolved scales. This is because scales at which the homogenization occurs are much smaller than the cloud model grid [below 1 cm versus tens or hundreds of meters; see discussions in Jensen and Baker (1989); Grabowski (1993); and Andrejczuk et al. (2004, 2006)]. As far as the turbulent mixing between a cloud and its environment is concerned, the timing of the homogenization is of primary importance because it results in evaporative cooling and typically the formation of negative (reversed) buoyancy (Grabowski 1993, 1995; Krueger 1993). This paper documents the development of a relatively simple approach designed to handle the disparity between spatial scales resolved by a cloud model and scales at which microscale homogenization takes place.

Various approaches have been developed in the past in an attempt to represent subgrid-scale structures in high-Reynolds-number turbulent flows. In large-eddy

* The National Center for Atmospheric Research is sponsored by the National Science Foundation.

Corresponding author address: Wojciech W. Grabowski, NCAR/MMM, P.O. Box 3000, Boulder, CO 80307-3000.
E-mail: grabow@ncar.ucar.edu

simulation (LES) of boundary layer clouds, an approach based on a subgrid-scale condensation scheme of Sommeria and Deardorff is often used [Sommeria and Deardorff (1977); see Bougeault (1981); Lewellen and Yoh (1993); and Table A1 in Siebesma et al. (2003)]. Sommeria and Deardorff (1977) showed that application of their scheme to a simulation of shallow nonprecipitating convection resulted in the vertical moisture transport that was enhanced and extended farther up when compared to the traditional bulk “all-or-nothing” scheme. Typically, the subgrid-scale condensation applies information provided by the modeled variances of the temperature and moisture fields and their correlation (cf. section 4 in Sommeria and Deardorff 1977). However, it is unclear if the subgrid-scale condensation scheme is capable of simulating the delayed evaporation associated with turbulent cloud–environment mixing. Such a delay can be captured in a natural way when a linear-eddy model of Kerstein (1988) is used to model subgrid-scale turbulent mixing as applied in studies discussed in Krueger (1993), Krueger et al. (1997), and Su et al. (1998). However, this approach is expensive and so far has not been used in cloud modeling using an atmospheric LES model. There is also a large body of literature in the combustion community devoted to the interactions between turbulent mixing and chemical reactions, such as techniques based on eddy-breakup and eddy-dissipation models [see section 1.9 in Peters (2000); Jeffery and Reisner (2006); and references therein]. A relatively simple approach advocated in this paper inevitably includes various elements of these previous techniques.

The next section briefly discusses the traditional bulk approach to cloud condensation and evaporation. The modified approach is presented in section 3. Section 4 illustrates the impact of the modifications on moist thermals rising from rest and realistic large-eddy simulations of a field of shallow convective clouds. Discussion and outlook are presented in section 5.

2. The bulk approach

For the nonprecipitating case, the thermodynamic grid-averaged equations in the anelastic system are (e.g., Grabowski and Smolarkiewicz 1990, and references therein)

$$\frac{\partial \theta}{\partial t} + \frac{1}{\rho_0} \nabla \cdot (\rho_0 \mathbf{u} \theta) = \frac{L_v \theta_e}{c_p T_e} C + D_\theta \quad (1a)$$

$$\frac{\partial q_v}{\partial t} + \frac{1}{\rho_0} \nabla \cdot (\rho_0 \mathbf{u} q_v) = -C + D_v \quad (1b)$$

$$\frac{\partial q_c}{\partial t} + \frac{1}{\rho_0} \nabla \cdot (\rho_0 \mathbf{u} q_c) = C + D_c, \quad (1c)$$

where θ , q_v , and q_c are the potential temperature, water vapor, and cloud water mixing ratios, respectively; $\rho_0(z)$ is the base-state density profile; $\theta_e(z)$ and $T_e(z)$ are the environmental potential temperature and temperature profiles; L_v and c_p denote the latent heat of condensation and specific heat at constant pressure, respectively; C is the condensation rate; and the last terms on the rhs of (1a)–(1c) represent subgrid-scale turbulent transport terms.

In the bulk model, the condensation rate C is defined by constraints that the cloud water can exist only in saturated conditions and that supersaturations are not allowed [all-or-nothing scheme; cf. (3) and (4) in Grabowski and Smolarkiewicz (1990)]. For the uniformly saturated and adiabatic air parcel (i.e., $q_v = q_{vs}$, where q_{vs} is the saturated water vapor mixing ratio, and $D_\theta = D_v = D_c \equiv 0$), the condensation rate C can be derived from the rate of change of the saturated water vapor mixing ratio (see the appendix). Such a condensation rate will be referred to as C^a , where the superscript a stands for “adiabatic.”

The system (1) is usually solved using the time-splitting technique (e.g., Grabowski and Smolarkiewicz 1990, and references therein). In this technique, advection and eddy diffusion are calculated first, and the values obtained from the advection–diffusion step are adjusted by the condensation–evaporation. The adjustment brings the grid box back to saturation, provided there is enough cloud water in the case of evaporation. The implicit relationship between the variables obtained in the first step and the final variables provides the condensation rate C [cf. (7) in Grabowski and Smolarkiewicz (1990)]. The condensation rate calculated in such a way will be marked as C^{sa} , where the superscript sa stands for the “saturation adjustment.” The saturation adjustment scheme can be easily made centered in time (cf. Grabowski and Smolarkiewicz 1996). Note that when saturation adjustment is applied, the grid box has to be saturated to contain any cloud water.

When the subgrid-scale structures of the thermodynamic fields exist, however, it is possible that the grid-averaged thermodynamic fields imply conditions below saturation and some cloud water does exist (cf. Sommeria and Deardorff 1977). Such conditions can occur, for instance, for a partially cloudy grid box, that is, when a part of the box is saturated and contains some cloud water, and the other part remains unsaturated and cloud-free. In fact, such a situation should be fairly typical for simulations of the turbulent mixing between a cloud and its dry environment when the model grid is much larger than scales at which small-scale homogenization occurs (cf. Andrejczuk et al. 2004, 2006).

3. The modified approach

The motivation for the modified approach is to improve representation of turbulent mixing between a cloud and its dry environment. Typically, the turbulent mixing leads to the evaporation of cloud water, so the emphasis here is on the formulation of the evaporation rate as already stated in the introduction. The picture of the turbulent mixing at Prandtl and Schmidt numbers close to unity is like that of the kinetic energy cascade, where larger eddies supply energy for smaller eddies, down to the Kolmogorov scale where the energy is dissipated by molecular processes. In this process, spatial scales of the scalar field decrease as the time progresses because of the development of smaller and smaller eddies, and the microscale homogenization (i.e., evaporation of cloud water) takes place once scales close to the Batchelor (and Kolmogorov) scale are reached (e.g., Jensen and Baker 1989; Grabowski 1993; Malinowski and Zawadzki 1993). Turbulent kinetic energy (TKE) can also be generated because of the evaporation of cloud water and buoyancy reversal at the cloud microscale (Grabowski 1993; Andrejczuk et al. 2004, 2006). The latter mechanism dominates when the large-scale TKE input is small (cf. Fig. 5 in Andrejczuk et al. 2004; Figs. 6 and 9–15 in Andrejczuk et al. 2006). It follows that moist processes within clouds can modify the classical picture because of the presence of buoyancy effects that are absent in the homogeneous and isotropic turbulence. However, recent tethered balloon observations suggest that the classical picture is valid down to the 10-cm scale (Siebert et al. 2006).

Using similarity arguments, Broadwell and Breidenthal (1982, their section 2) proposed the following equation describing the evolution of the spatial scale λ of the filaments of a conserved scalar field¹ during turbulent mixing:

$$\frac{d\lambda}{dt} = -\alpha\epsilon^{1/3}\lambda^{1/3}, \quad (2)$$

where ϵ is the dissipation rate of the TKE and α is a proportionality constant that has to be determined. If U and L are the velocity and spatial scale of large-scale (resolved) eddies that serve as a source of energy for the cascade, then $\epsilon \sim U^3/L$.

The time $\tau(l)$ required to break the initial-scale L

¹ The scale λ can be formally defined in a similar manner as the Taylor microscale using the scalar field ψ in place of the velocity field, that is, as $\langle \psi^2 \rangle^{1/2} / \langle \nabla \psi^2 \rangle^{1/2}$, where angle brackets depict average over a volume much larger than λ [e.g., see Eq. (8) and Figs. 1–3 and 9 in Andrejczuk et al. (2004)]. See also illustration of cloud filaments in Fig. 4 of Andrejczuk et al. (2006).

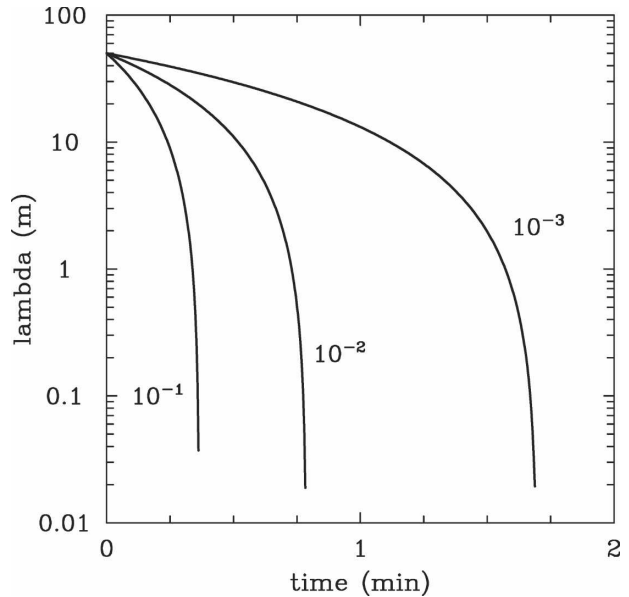


FIG. 1. Evolution of the filament width λ predicted by (2) for different dissipation rates. Each line is labeled by the dissipation rate in $\text{m}^2 \text{s}^{-3}$.

down to the much smaller-scale l might be estimated by integrating (2). The result is the following (Broadwell and Breidenthal 1982):

$$\tau(l) = \frac{3}{2} \frac{1}{\alpha} \frac{L}{U} \left[1 - \left(\frac{l}{L} \right)^{2/3} \right] \approx \frac{3}{2} \frac{1}{\alpha} \frac{L}{U} = \frac{3}{2} \frac{1}{\alpha} \left(\frac{L^2}{\epsilon} \right)^{1/3} \quad (3)$$

for $l \ll L$.

Since it is usually assumed that eddies lose a significant fraction of their energy in a single eddy turnover time L/U , it can be assumed that $\alpha \approx 1$. It can also be shown that the linear-eddy model implies $\alpha = 1.8$ (S. Krueger 2006, personal communication). In such a case, (3) predicts that the time τ is about three quarters of the eddy turnover time. In simulations discussed in section 4, $\alpha = 1.8$ is assumed.

Figure 1 illustrates prediction of (2) for the case of mixing events with $L = 50$ m and three different eddy dissipation rates: $\epsilon = 10^{-3}$, 10^{-2} , and $10^{-1} \text{ m}^2 \text{ s}^{-3}$. The lowest value corresponds to low turbulence intensity as observed in convective clouds (i.e., near the cloud base), whereas the highest value may be considered the upper limit of the observed dissipation rates in the regions of active entrainment and mixing between a cumulus cloud and its environment (cf. MacPherson and Isaac 1977; Siebert et al. 2006). As the figure shows, it takes about 20 s to complete the mixing for $\epsilon = 10^{-1} \text{ m}^2 \text{ s}^{-3}$, whereas close to two minutes is needed for the case of $\epsilon = 10^{-3} \text{ m}^2 \text{ s}^{-3}$. When plotted on the log scale, the mixing predicted by (2) progresses slowly initially

and accelerates as λ decreases: for $\epsilon = 10^{-3} \text{ m}^2 \text{ s}^{-3}$, it takes more than 1 min to decrease the scale from 50 to 5 m, and only a few seconds to proceed from 10 to 1 cm.

Equation (2) is used as a foundation to model the subgrid-scale homogenization process. It is done by expanding (3) in the following way: i) advection of the scale λ is allowed, ii) Reynolds averaging to represent subgrid-scale transport similarly as in (1) is added, and iii) source–sink term of λ is included. The resulting conservation equation is

$$\frac{\partial \lambda}{\partial t} + \frac{1}{\rho_0} \nabla \cdot (\rho_0 \mathbf{u} \lambda) = -\alpha \epsilon^{1/3} \lambda^{1/3} + S_\lambda + D_\lambda, \quad (4)$$

where S_λ is the source–sink term and D_λ is the subgrid transport term. The subgrid-scale transport term can be modeled in the same way as corresponding terms in (1). The dissipation rate of the TKE ϵ is represented in a standard way; that is,

$$\epsilon = c_\epsilon \frac{E^{3/2}}{\Lambda}, \quad (5)$$

where E is the model-predicted TKE, $\Lambda = (\Delta x \Delta y \Delta z)^{1/3}$ [$\Lambda = (\Delta x \Delta z)^{1/2}$ in 2D]; Δx , Δy , and Δz are model grid length in x , y , and z direction, respectively; and c_ϵ is a constant (e.g., Klemp and Wilhelmson 1978; Margolin et al. 1999).

The source–sink term S_λ considers three processes that affect the scale λ . These are (a) the formation of cloudy volumes due to grid-scale condensation; (b) the disappearance of cloudy volumes due to complete evaporation of cloud water; and (c) the homogenization of a cloudy volume. Since it is assumed that condensation due to saturation adjustment occurs always over the entire grid box, (a) is represented by simply resetting current value of λ to the size comparable to the size of the grid box, say, Λ . Complete evaporation of cloud water [i.e., process (b)] is represented by resetting λ to zero. Finally, microscale homogenization of the cloudy grid box (i.e., homogenization that results in a saturated grid box containing some cloud water) is represented by setting $\lambda = \Lambda$. These processes can be schematically represented as

$$(a): \lambda \rightarrow \Lambda \quad \text{if} \quad C^{sa} > 0 \quad (6a)$$

$$(b): \lambda \rightarrow 0 \quad \text{if} \quad q_c = 0 \quad (6b)$$

$$(c): \lambda \rightarrow \Lambda \quad \text{if} \quad \lambda < \lambda_0 \quad \text{and} \quad q_c \neq 0, \quad (6c)$$

where λ_0 is the threshold value of λ that represents scale at which molecular homogenization occurs (e.g., the Batchelor microscale). In the computational example used in the next section, $\lambda_0 = 1 \text{ cm}$ has been assumed.

In the modified approach, the condensation rate C applied in (1) is calculated depending whether the saturation adjustment predicts condensation or evaporation, and, in the case of evaporation, depending on the size of filaments as predicted by (4).² When the saturation adjustment predicts condensation, the rate applied in (1) is the same as in the traditional bulk model; that is,

$$C = C^{sa} \quad \text{when} \quad C^{sa} > 0. \quad (7a)$$

When saturation adjustment predicts evaporation, the saturation adjustment is applied only if $\lambda \leq \lambda_0$ or $\lambda = \Lambda$; otherwise adiabatic rate is used. In the latter case, the fraction of the grid box covered by cloudy air β has to be considered because the adiabatic rate applies only to the cloudy part of the grid box (cf. Brenguier and Grabowski 1993). In summary, in the case of evaporation (i.e., $C^{sa} < 0$), the rate applied in (1) is given by

$$C = \beta C^a \quad \text{if} \quad \Lambda > \lambda > \lambda_0, \quad (7b)$$

$$C = C^{sa} \quad \text{if} \quad \lambda \leq \lambda_0 \quad \text{or} \quad \lambda = \Lambda. \quad (7c)$$

Note that the rate applied in (7b) might be either positive or negative depending on the vertical velocity (i.e., condensation and evaporation are both possible).

In general, partial cloudiness β should be independently predicted by the model. However, β is only required in (7b), which has already been proposed based on relatively simple arguments. It follows that using a crude estimate of the fractional cloudiness in (7b) should be sufficient. Such an estimate can be derived based on the following argument. If the grid box under consideration is assumed to consist of both cloudy and cloud-free parts, then the mean water vapor mixing ratio q_v is a linear combination of the saturated water vapor mixing ratio for the cloudy part and the unsaturated mixing ratio for the cloud-free part. Furthermore, if the temperature difference between the cloudy and cloud-free parts is assumed to be small (i.e., the volume-averaged temperature provides a reasonable estimate for both the cloudy and cloud-free air temperature), and if the water vapor mixing ratio for the cloud-free part is approximately equal to that of the

² Note that such an approach implicitly assumes that locally the evaporation rate due to parameterized mixing is larger (in the absolute sense) than the condensation rate due to the resolved vertical motion. In other words, a situation when saturation adjustment predicts condensation but there is still some evaporation due to parameterized mixing occurs infrequently. Figures 2–5 in Grabowski and Smolarkiewicz (1990) show the condensation rate due to vertical motion and the evaporation rate due to numerical diffusion, with the evaporation rate significantly larger than the condensation rate.

environment at this level q_v^e , then the volume-averaged q_v can be approximated as

$$q_v \approx \beta q_{vs}(T) + (1 - \beta)q_v^e, \quad (8)$$

or, by dividing by $q_{vs}(T)$,

$$\text{RH} \approx \beta + (1 - \beta)\text{RH}^e, \quad (9)$$

where RH and RH^e are the relative humidities of the grid box and the environment, respectively. With additional limiting to avoid unphysical values, the cloud fraction can thus be approximated from (9) as

$$\beta = \max \left[0, \min \left(1, \frac{\text{RH} - \text{RH}^e}{1 - \text{RH}^e} \right) \right]. \quad (10)$$

The environmental relative humidity RH^e can be taken either from the input sounding or by appropriate averaging of the model data at a given level (e.g., taking into account cloud-free points only). Note that such estimates neglect modifications of the immediate cloud environment by detrainment (cf. Radke and Hobbs 1991).

In summary, the modified bulk approach adds one extra conservation Eq. (4) to the set of model equations and applies condensation rate as given by (7) combined with (10) and (A5). Computational examples presented in the next sections illustrate the effect of the modified approach on cloud dynamics.

4. Computational examples

The modified bulk model was included in the anelastic semi-Lagrangian–Eulerian cloud model EULAG documented in Smolarkiewicz and Margolin (1997; model dynamics), Grabowski and Smolarkiewicz (1996; model thermodynamics), and Margolin et al. (1999; subgrid-scale model). The simulations presented here were performed using the Eulerian version of the model. Two different modeling tests are discussed below. The first one considers 2D rising thermals and is used to illustrate general aspects of the proposed extension of the bulk scheme. In the second test, EULAG is setup to simulate quasi-steady-state trade wind shallow nonprecipitating convection observed during the Barbados Oceanographic and Meteorological Experiment (BOMEX; Holland and Rasmusson 1973) and recently used in the model intercomparison study described in Siebesma et al. (2003).

a. Simulations of 2D rising thermals

The 2D test is similar to the problem discussed in Grabowski and Clark (1991, 1993a,b). Moist thermals,

initially at rest, rise in a stably stratified unsaturated environment (static stability of $1.0 \times 10^{-5} \text{ m}^{-1}$, relative humidity of 10%) because of the initial buoyancy perturbation. Rising motion and accompanying adiabatic cooling lead to condensation. Subsequent evolution results in entrainment and mixing between the saturated cloudy air within the thermal and its unsaturated environment. The initial buoyancy anomaly is due to the excess of the water vapor within the initial perturbation. The initial perturbation is circular, with a center at $(x, z) = (0, 1200 \text{ m})$. Saturation is assumed within 400 m radius, and a gradual transition between the saturated perturbation and the environment is facilitated by relative humidity linearly decreasing from 100% at the radius of 400 m to 10% at 500 m. To provide excitation for the interfacial instabilities, random perturbations are added to the temperature and water vapor mixing ratio at $t = 0$ within the 500-m radius (amplitudes equal to 0.05 K and 0.1 g kg^{-1}). The model domain is $[-2500 \text{ m}, 2500 \text{ m}] \times [0, 5000 \text{ m}]$. Boundary conditions are periodic in x and free-slip rigid lid in z . Simulations are performed using the spatial grid length (the same in x and z) of 5, 10, 50, and 100 m. The time steps used in the simulations are 0.2, 0.5, 3, and 5 s, respectively. Only results from simulations applying 10 and 50 m grid lengths are presented because they sufficiently illustrate the impact.

Figures 2 and 3 show the results from simulations using a 50-m grid at $t = 5$ and 10 min and using either the standard bulk model (Fig. 2) or the bulk model with the evaporation of cloud water suppressed [i.e., $C = \max(0, C^{sa})$ in (1); Fig. 3]. As far as the turbulent mixing between the thermal and its environment is concerned, the two cases can be considered as opposite limits. The standard model assumes instantaneous subgrid-scale homogenization and thus can be thought as representing the case of infinitely high turbulence intensity (i.e., $\epsilon \rightarrow \infty$). The model with suppressed evaporation of cloud water, on the other hand, corresponds to the case with no subgrid-scale homogenization (i.e., $\epsilon = 0$)³. At $t = 5$ min, the differences between the two simulations are minor, with smaller extent of the cloud water and colder temperature just above the thermal in the case of the standard bulk model, both resulting from turbulent mixing and subsequent evaporation of cloud water. The differences at $t = 10$ min are significant. In contrast to the case of suppressed evaporation,

³Note that limiting the condensation rate to positive values excludes not only evaporation due to turbulent mixing, but also the grid-scale evaporation due to resolved subsidence as well. The latter can be argued of secondary importance for the problem at hand.

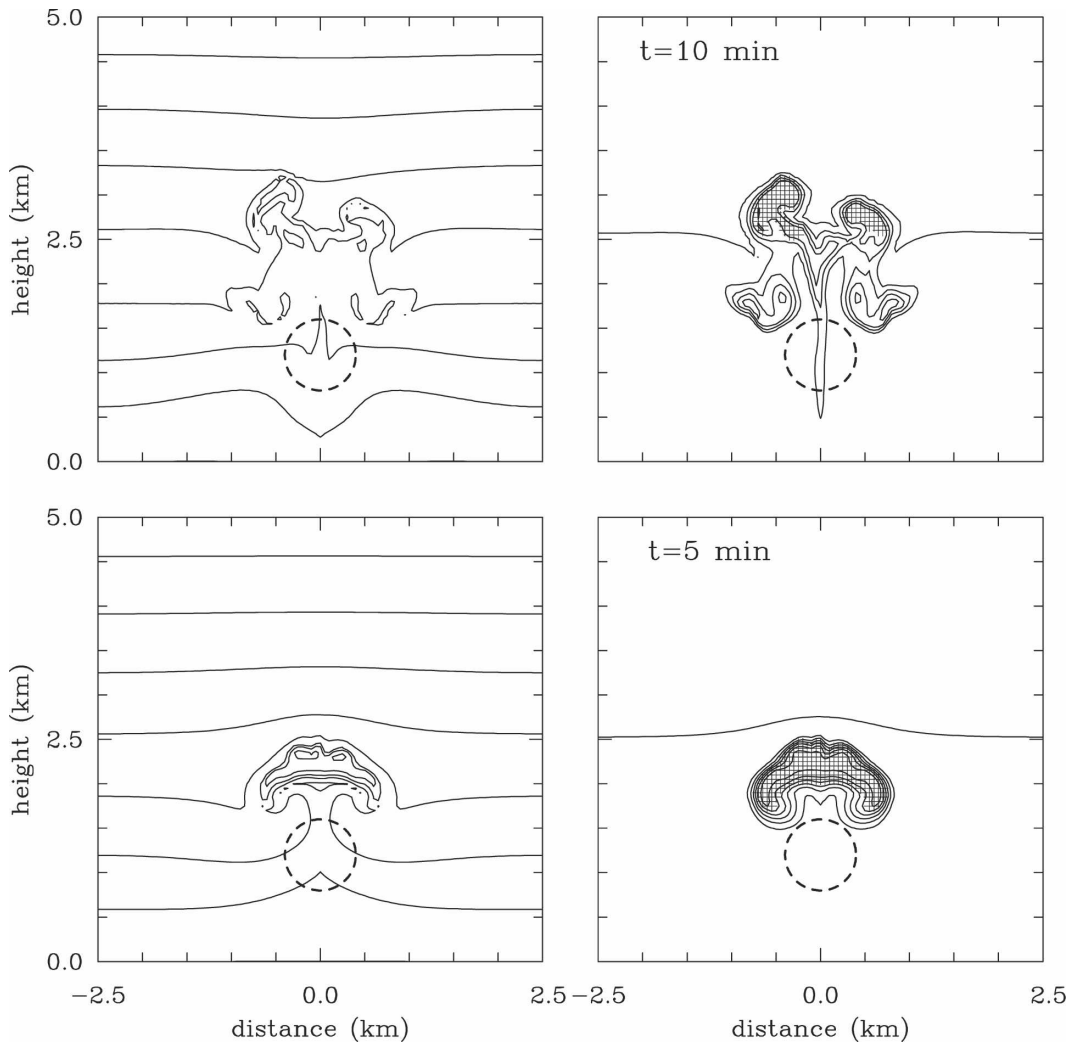


FIG. 2. Fields of the (left) potential temperature and (right) water vapor mixing ratio for rising thermal calculations using the standard bulk model with a grid length of 50 m. Results are shown for (bottom) $t = 5$ min and (top) $t = 10$ min. Regions with the cloud water mixing ratio larger than 0.01 g kg^{-1} are hatched. Position of the initial circular perturbation is shown by thick dashed line.

the standard model predicts only a small area near the top of the thermal that still contains cloud water. Moreover, the cloud top is about 500 m lower in the standard bulk case than in the no-evaporation case. The wake of the thermal contains cloud water only when evaporation of cloud water is suppressed.

Figures 4, 5, and 6 show results from similar simulations, but using the modified approach and assuming $\text{RH}^c = 10\%$ in (10). For illustration, we first show results from simulations where the dissipation rate ϵ applied in (4) is assumed constant, rather than being predicted by the TKE model. Figure 4 is for $\epsilon = 10^{-4} \text{ m}^2 \text{ s}^{-3}$, whereas Fig. 5 is for $\epsilon = 10^{-1} \text{ m}^2 \text{ s}^{-3}$. As argued in the last section, $\epsilon = 10^{-4} \text{ m}^2 \text{ s}^{-3}$ can be taken as the minimum value because of the TKE production at

small scales during turbulent mixing between cloudy and cloud-free air (see Andrejczuk et al. 2004, 2006). The value $\epsilon = 10^{-1} \text{ m}^2 \text{ s}^{-3}$ is larger than the upper limit of dissipation rates observed in continental cumuli by MacPherson and Isaac (1977).

For the case of $\epsilon = 10^{-4} \text{ m}^2 \text{ s}^{-3}$ (Fig. 4) the results are fairly similar to the no-evaporation case (Fig. 3). The most significant difference is the lack of cloud water in the wake at $t = 10$ min in Fig. 4. The case with $\epsilon = 10^{-1} \text{ m}^2 \text{ s}^{-3}$ (Fig. 5) is similar to the standard model (Fig. 2), except that the cloud top is significantly higher at $t = 10$ min. In fact, the cloud top is close to the case with suppressed evaporation (Fig. 3). These results are consistent with the anticipated impact of the modified approach on cloud dynamics when model spatial resolu-

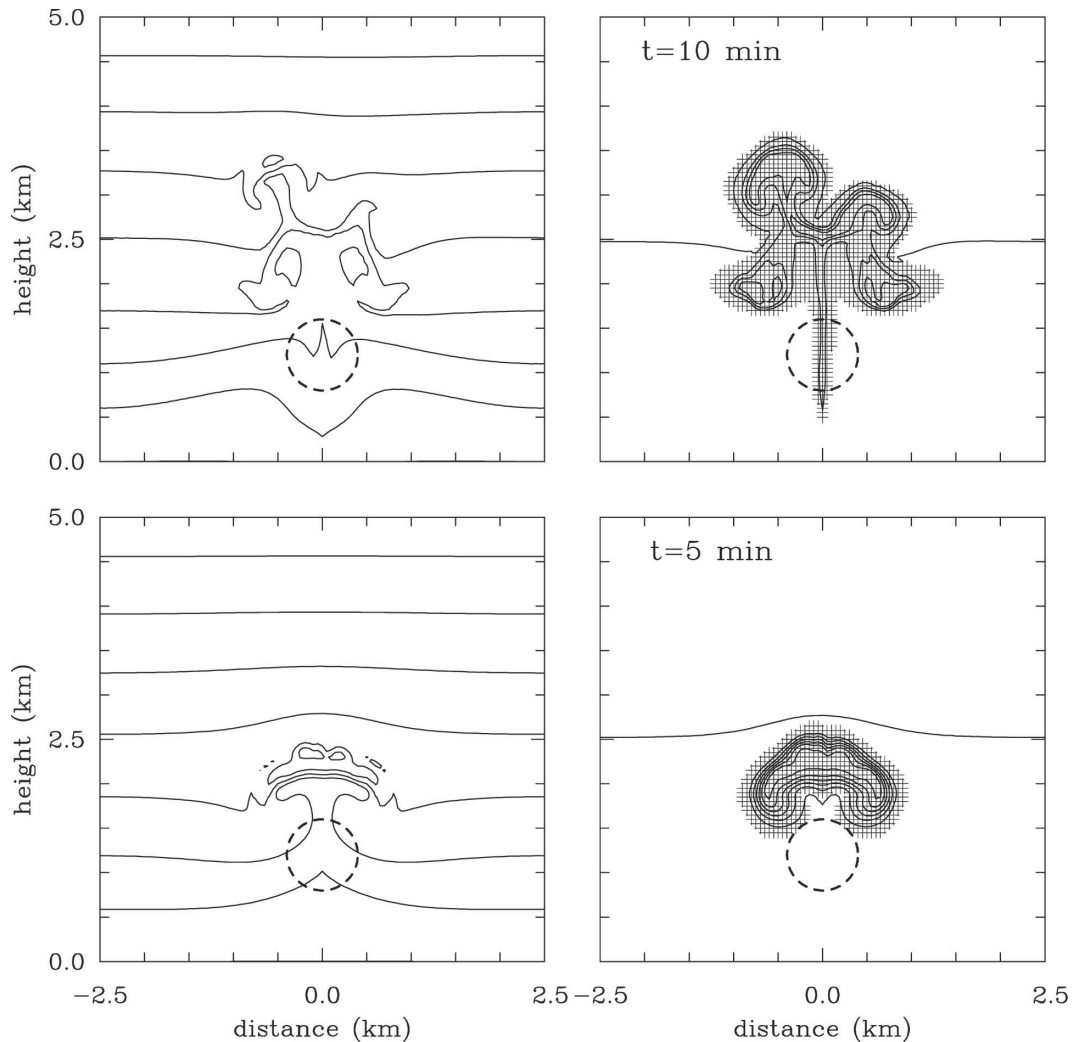


FIG. 3. Same as in Fig. 2, but for the standard bulk model with suppressed evaporation of cloud water.

tion is relatively low and most of the entrainment and mixing is handled by the subgrid-scale model.

The results from the simulation where ϵ is predicted using the local value of the TKE via (5) are shown in Fig. 6. Since the subgrid-scale model does not consider generation of TKE by evaporation of cloud droplets at the cloud microscale (Andrejczuk et al. 2004, 2006), ϵ applied in (4) is limited as $\max(10^{-5}, \epsilon')$, where ϵ' is predicted by (5). However, in the particular test considered here, almost indistinguishable results are obtained without such a limitation. Figure 6 should be compared with Fig. 2, which shows the standard bulk model results. The differences are obvious. With the modified approach, there is more cloud water left at $t = 10$ min, and the cloud top is significantly higher, close to the no-evaporation case (Fig. 3) and consistent with constant- ϵ simulations (Figs. 4 and 5). Similar differ-

ences between the original and modified approach are obtained in simulations applying a grid length of 100 m (not shown).

Arguably, the differences between the original and modified approaches should diminish once sufficiently high spatial resolution is applied. To illustrate this point, Fig. 7 shows results for $t = 10$ min from the original and modified bulk models using a model grid length of 10 m. Although the two model configurations lead to different realizations of interfacial instabilities, the cloud-top height is similar in both cases, and there is still some cloud water left in the wake. However, the volumes with at least a trace of cloud water (i.e., the hatched area in Fig. 7) differ significantly (~ 2400 versus ~ 3700 grid points in the original and modified approach, respectively). It is also interesting to note that the 10-m-gridlength simulations allow thermals to reach

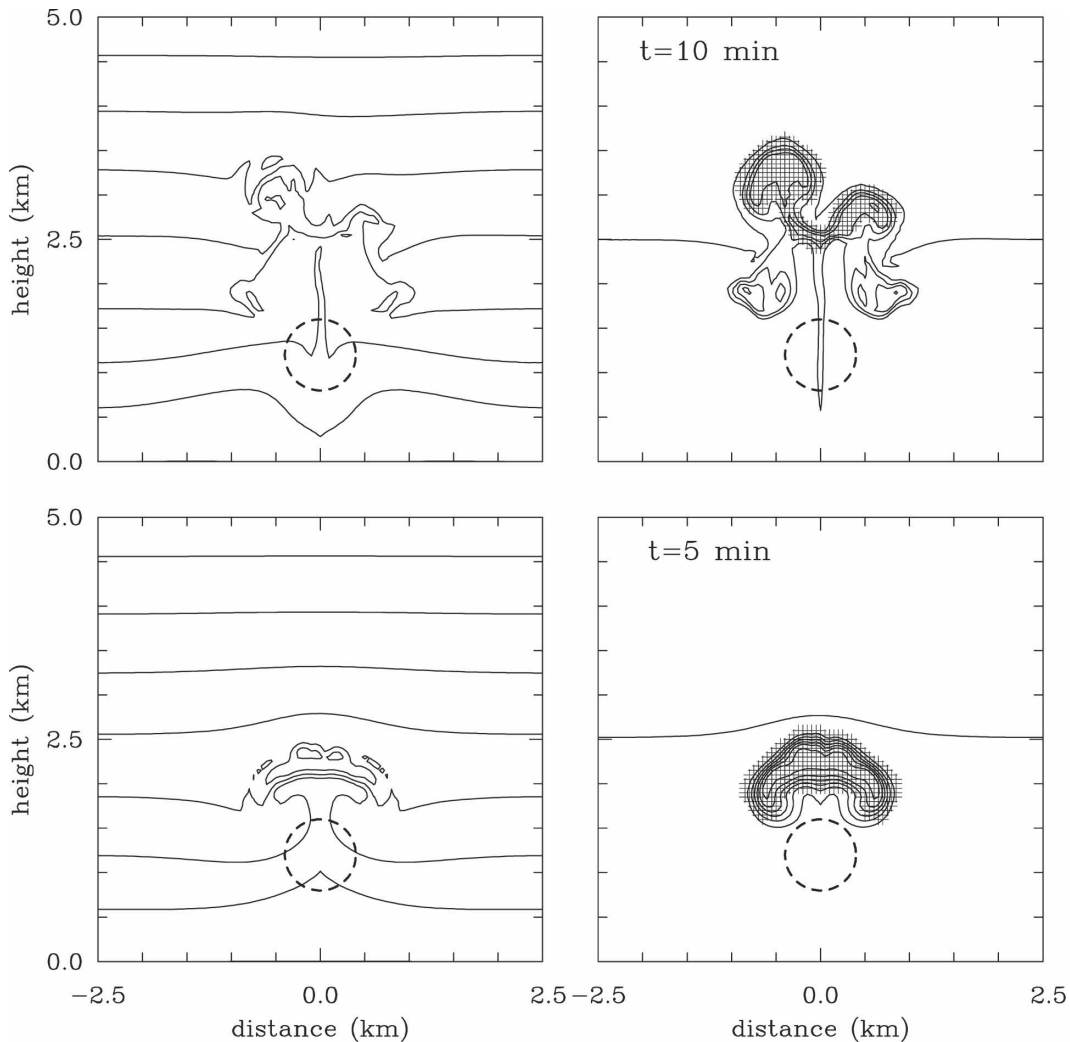


FIG. 4. Same as in Fig. 2, but with the modified bulk model applying the constant dissipation rate $\epsilon = 10^{-4} \text{ m}^2 \text{ s}^{-3}$.

approximately the same height as in the 50-m simulations using the modified approach (about 3.5 km). Similar conclusions are reached by comparing results from simulations applying model grid length of 5 m (not shown).

b. Simulations of a field of shallow convective clouds observed in BOMEX

In the BOMEX case (see Siebesma et al. 2003; hereafter S03), the 1.5-km-deep trade wind convection layer overlays a 0.5-km-deep mixed layer near the ocean surface and is covered by a 500-m-deep trade wind inversion layer. The cloud cover is about 10% and quasi-steady conditions are maintained by the prescribed large-scale subsidence, large-scale moisture advection, surface heat fluxes, and radiative cooling. The model setup is exactly as described in S03, except that a larger

horizontal domain is used (128×128 rather than 64×64). The horizontal and vertical grid length is 100 m and 40 m, respectively, and the model time step is 3 s. In the modified approach, RH^e in (10) is taken as the horizontally averaged RH at a given level. This seems appropriate considering the low cloud fraction in these simulations. The model is run for 6 h and snapshots of model results archived every 4 min are used in the analysis.

With the original bulk approach, EULAG's results fall within the spread of model results presented in S03 (see figures below). The modified approach, on the other hand, results in significant differences, with some of results outside the spread of S03 results. Figure 8 shows evolutions of the total cloud cover (defined as the fraction of model columns with a nonzero cloud water anywhere in the column) and mean liquid water

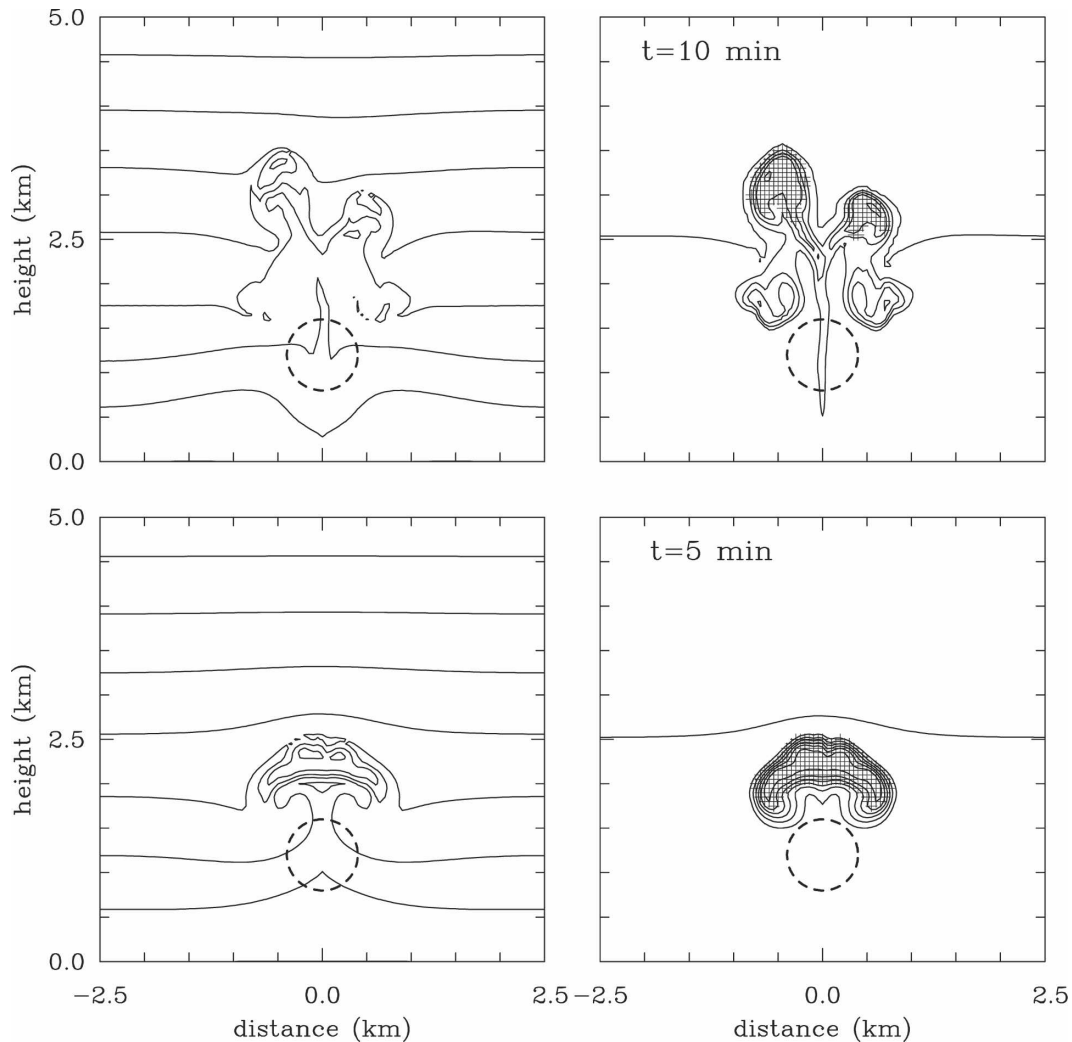


FIG. 5. Same as in Fig. 2, but with the modified bulk model applying the constant dissipation rate $\epsilon = 10^{-1} \text{ m}^2 \text{ s}^{-3}$.

path (LWP). Figure 8 should be compared with Fig. 2 in S03. The figure shows that the modified approach affects both the cloud cover and the LWP. The impact on the cloud cover is difficult to quantify, as the difference during the period considered as quasi-steady in S03, that is, hours 2 to 6, is virtually zero (around 0.13 in both cases). In contrast, the difference between the averaged LWPs for the same period is large (i.e., almost a factor of two; 6.9 versus 13.1 g m^{-2}).

Figure 9 shows the profiles of the cloud fraction averaged over hours 2–6. Corresponding profiles of cloud water mixing ratio as well as the water vapor profiles at hours 2 and 6 (i.e., at the start and at the end of the quasi-steady period according to S03) are shown in Fig. 10. The two figures are to be compared with Figs. 3 and 6 in S03. Figures 9 and 10 illustrate that the standard model results fall within the limits of the ensemble of

simulations discussed in S03, and that the water vapor profiles change little between hours 2 and 6. The modified approach, on the other hand, results in the cloud field that is deeper (consistent with higher LWPs) with larger cloud fractions and liquid water contents in the upper half of the cloud layer. These changes of the cloud field lead to more significant modifications of the water vapor profiles between hours 2 and 6. The changes of the water vapor profiles are consistent with the changes of the resolved total water flux profiles, which in the standard simulation are close to those shown in S03 (Fig. 4a therein), with values around 125 and 75 W m^{-2} for heights of 1 and 1.5 km, respectively. In the modified approach, the total water flux is up to 50 W m^{-2} higher in the layer between 1 and 2 km (not shown). The enhanced cloud activity in this layer is consistent with the higher cloud fraction and higher

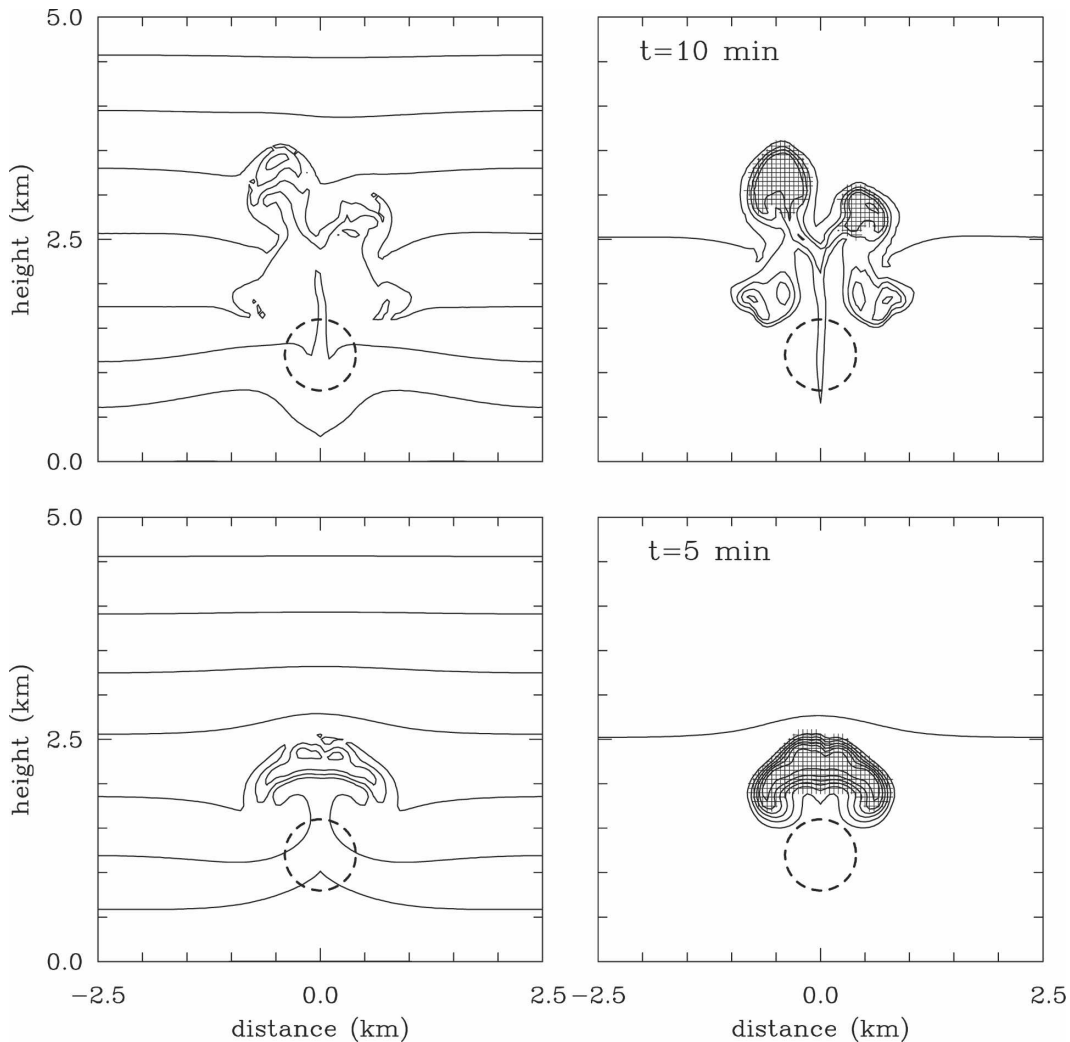


FIG. 6. Same as in Fig. 2, but with the modified bulk model applying the dissipation rate as predicted by (5).

cloud water content, as well as the change in the water vapor profiles documented in Figs. 9 and 10.

In summary, the impact of the modified bulk approach on a field of shallow convective clouds is consistent with the effect on cloud dynamics illustrated in the previous section. It is also consistent with the effect of a subgrid-scale condensation scheme of Sommeria and Deardorff (1977), as documented in their section 6. However, since two of the models applied in S03 study did include the Sommeria–Deardorff scheme (see table A1 in S03), and some results from the modified model here are outside the spread of results documented in S03 (notably LWP, cloud fraction, and cloud water content), it seems that the approach proposed in this paper results in a significantly stronger effect than the one due to the Sommeria–Deardorff approach. Moreover, the results of the cloud field simulations (but not the 2D

thermal simulations) appear sensitive to the selection of α in (4). For instance, taking $\alpha = 1$ rather than 1.8 (which approximately doubles the delay time for the small-scale homogenization with all other conditions unchanged) further increases LWP and cloud profiles. This aspect, together with the role of model spatial resolution (as illustrated in simulations of 2D moist thermals) needs to be investigated in follow-up studies.

5. Summary and outlook

Modeling of subgrid-scale processes is an important aspect of the simulation of high-Reynolds-number atmospheric flows in general, and cloud processes in particular (e.g., Sommeria and Deardorff 1977; Bougeault 1981; Lewellen and Yoh 1993; Krueger 1993; Krueger et al. 1997; Jeffery and Reisner 2006). This especially

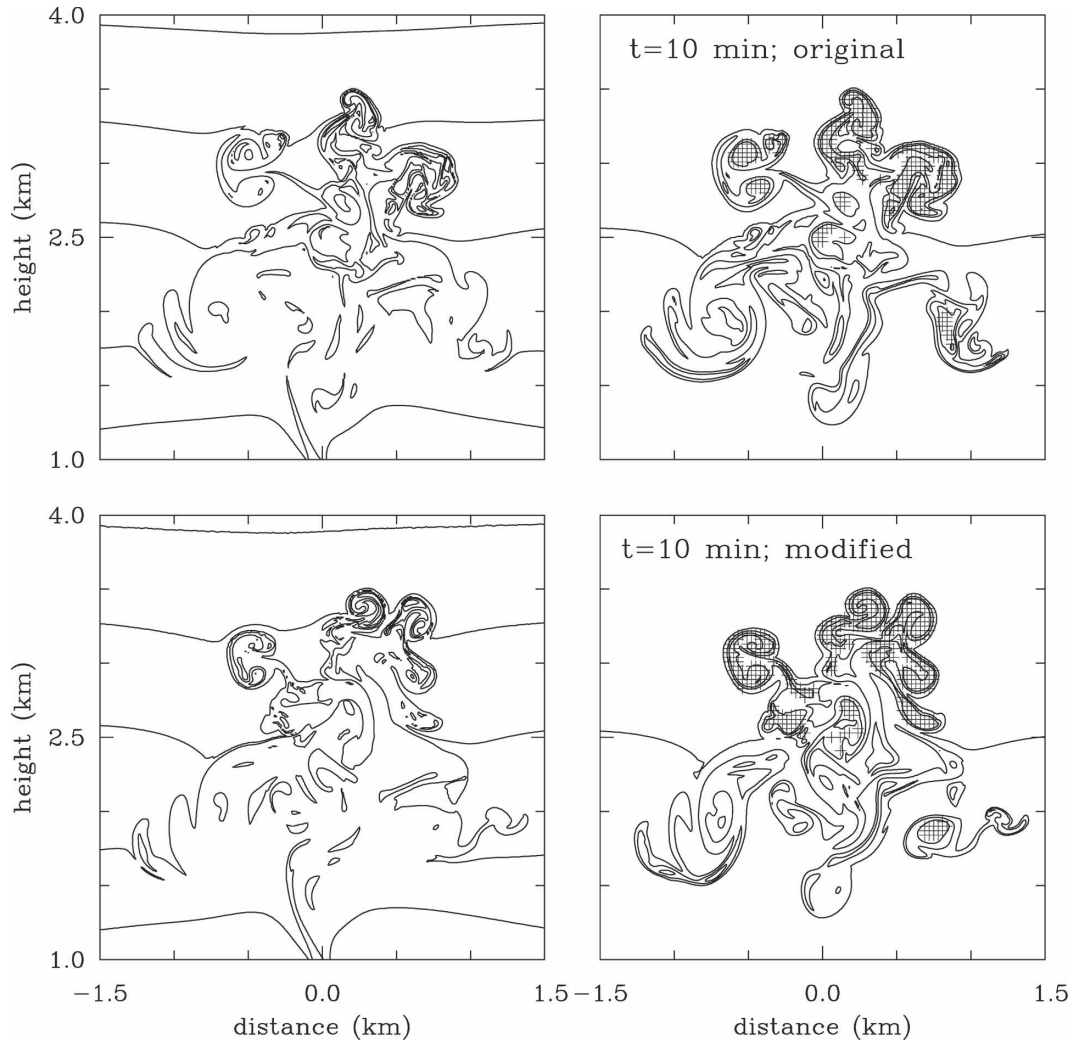


FIG. 7. Fields of the (left) potential temperature and (right) water vapor mixing ratio at $t = 10$ min for rising thermal calculations using the (top) standard bulk model and (bottom) modified model with a model grid length of 10 m. Regions with the cloud water mixing ratio larger than 0.01 g kg^{-1} are hatched. Only the central part of the domain is shown.

applies to the case of the turbulent mixing between a cloud and its unsaturated environment because the buoyancy resolved over model grid (usually tens or hundreds of meters) depends critically on the level of grid-box homogenization. The intention of this paper is to demonstrate the importance of this problem and to show that the traditional bulk approach is not appropriate for models with relatively low spatial resolutions (grid lengths of several tens of meters or larger) because it assumes instantaneous homogenization over model-resolved scales.

The approach proposed in this paper is based on a simple model of scale collapse of a scalar field during high-Reynolds-number turbulent mixing. The model attempts to account for the disparity between scales

resolved by the dynamical model and scales at which microscale homogenization takes place. The condensation of water vapor due to model-resolved rising motion results in fully saturated grid boxes that are characterized by the filament width $\lambda = \Lambda$, where Λ is the size of the grid box. Near the cloud–environment interface, where the turbulent mixing takes place, partially cloudy grid boxes are present. Local values of λ , as predicted by (4), determine whether a partially cloudy grid box is at the stage of turbulent mixing advanced enough to allow microscale homogenization. If the filament size is still too large to allow microscale homogenization, the adiabatic condensation rate is applied to the cloudy part of the grid box. Microscale homogenization is possible only if the filament size λ has already

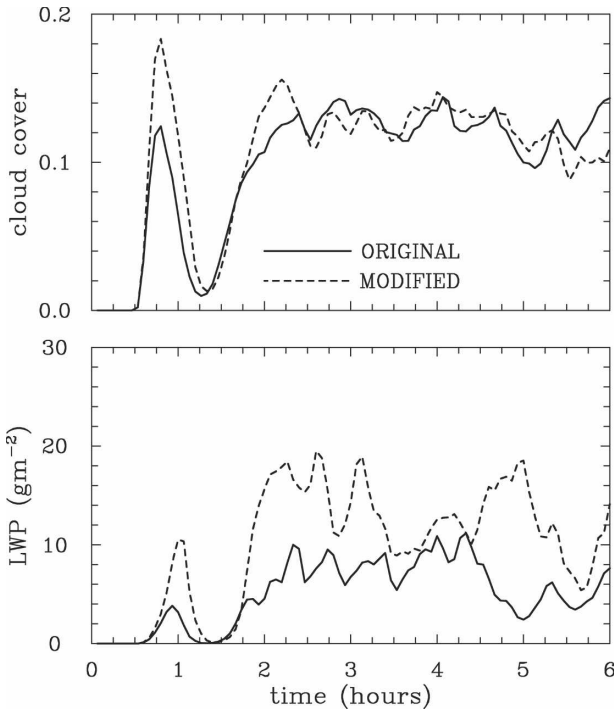


FIG. 8. Evolutions of the (top) cloud cover and (bottom) LWP in BOMEX simulations using either the original (solid lines) or the modified (dashed lines) approaches.

collapsed to a threshold value of, say, 1 cm. These two extreme situations usually predict dramatically different grid box-averaged buoyancy.

The adiabatic rate applied within partially cloudy grid boxes recognizes the condensation–evaporation of

cloud water due to ascending–descending motions resolved over the model grid. Considerable time may elapse before microscale homogenization takes place (cf. Fig. 1), and the amount of cloud water present inside cloudy filaments may change significantly during this time. Krueger (1993) suggests that this effect plays an important role in the entrainment in stratocumulus clouds because partially cloudy parcels containing dry air from above the inversion are able to move away from the interface before mixing is completed, and the amount of the condensed water available for evaporation is significantly reduced during this time.

In agreement with the impact documented in Sommeria and Deardorff (1977), incorporation of the approach described in this paper into an anelastic small-scale model leads to a significant modification of the traditional bulk model results. In 2D rising thermal simulations, the modified approach resulted in thermals reaching farther up when 100- and 50-m grid lengths were applied. With 5- and 10-m grid lengths, the impact resulted in merely different realizations of the thermal shape, with some reduction of the cloudy volume. In 3D simulations of a field of shallow cumuli observed in BOMEX and used in the model intercomparison study described in Siebesma et al. (2003), the impact on the mean liquid water path, cloud depth, and cloud water content, as well as on the transport of the total water across the cloud layer was significant when grid lengths of 100 m (40 m) in the horizontal (vertical) were used. BOMEX results (unlike 2D rising thermal results) also showed significant sensitivity to the constant α in the rate of filament-scale collapse (3). The value used in the

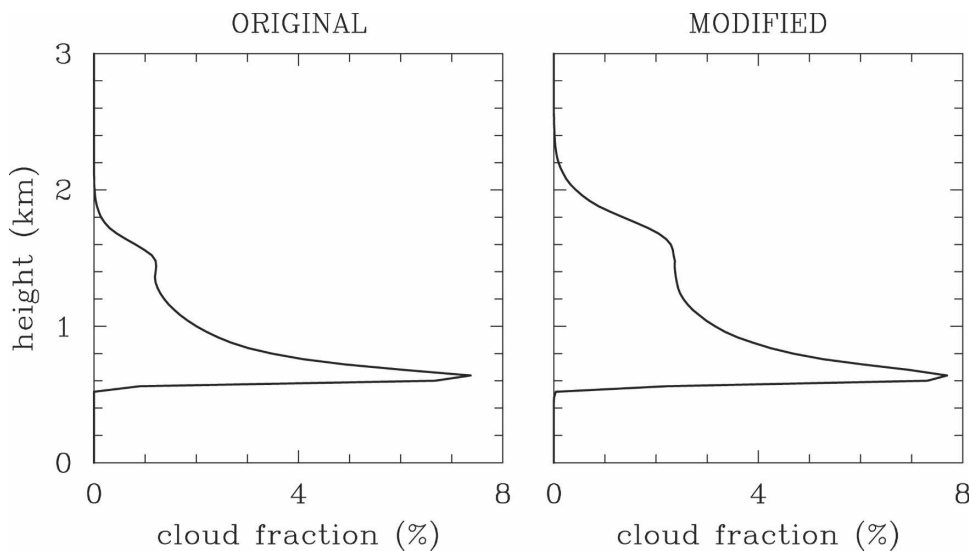


FIG. 9. Profiles of the cloud fractions (4-h averages) in BOMEX simulations using either the (left) original or (right) modified approaches.

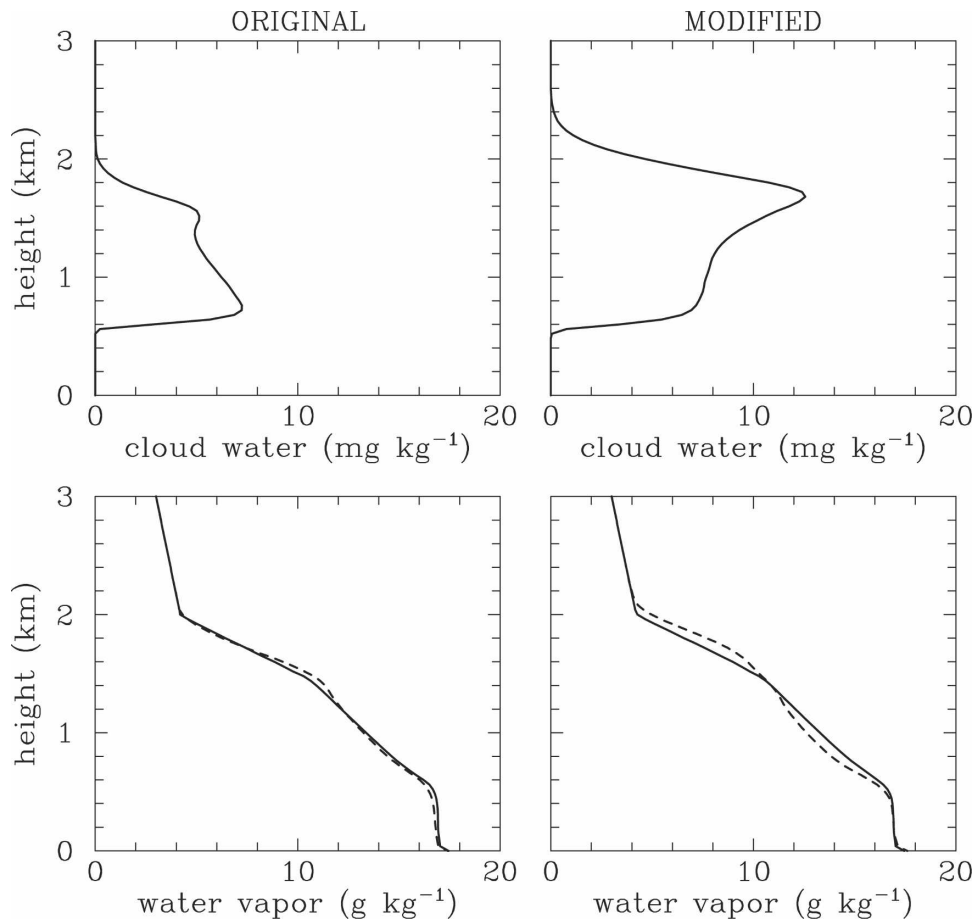


FIG. 10. Profiles of the (top) cloud water mixing ratio (4-h averages) and (bottom) water vapor mixing ratios at (solid lines) 2 h and (dashed lines) 6 h in BOMEX simulations using either the (left) original or (right) modified approaches.

current study ($\alpha = 1.8$) was suggested by S. Krueger (2006, personal communication) and it is based on theoretical arguments applying the linear-eddy model of Kerstein (1988). More studies using the linear-eddy model as well as direct numerical simulations of the type discussed in Andrejczuk et al. (2004, 2006) are needed to provide reliable estimate of this parameter. BOMEX simulations should also be repeated using significantly higher spatial resolutions, down to 10 m as in the 2D rising thermal case.

The modification of the traditional bulk model presented in this paper contains significant simplifications. First, the model does not consider partially cloudy grid boxes explicitly. To do so, the model has to predict partial cloudiness β that is only diagnosed in the current model. More importantly, representation of the scale collapse during turbulent mixing, based on similarity arguments of Broadwell and Breidenthal (1982), is a simplification as well. This is because the approach excludes subgrid-scale variability of λ , TKE, ϵ , and the

like. As a result, the transition from a heterogeneous partially cloudy grid box into an already homogenized grid box happens during a single model time step. In contrast, a gradual transition is expected in nature, as various parts of the grid box volume may homogenize locally at different times. Such effects, however, can only be considered in more elaborate approaches, for instance, by applying probability density functions describing subgrid-scale variability (e.g., Jeffery and Reisner 2006 and references therein) or by using the linear-eddy model of Kerstein (1988; see Krueger 1993; Krueger et al. 1997; Su et al. 1998).

This paper points toward the need of more realistic treatment of partially cloudy grid boxes in cloud models, especially in the context of cloud entrainment and mixing. This aspect has potentially significant implications not only for cloud dynamics as illustrated herein, but for cloud microphysics as well. The role of cloud microphysics in the clouds-in-climate problem has attracted considerable attention because of the impact of

microphysical processes on the cloud albedo and on the hydrologic cycle (see a review and discussion in Grabowski 2006). At the same time, numerical models that are applied to investigate these effects (either LES models or cloud-resolving models, CRMs) apply relatively coarse horizontal grid lengths, typically around 100 m for LES models and 1–3 km for CRMs. Because such models assume instantaneous homogenization of thermodynamic fields within each grid box, representation of microphysical processes associated with cloud entrainment and mixing is highly uncertain [see discussions in Grabowski (2006) and Andrejczuk et al. (2006)]. This issue is important because it is well established from aircraft observations that clouds are typically strongly diluted by entrainment. The approach advocated in this paper may provide a potentially useful strategy to subgrid-scale turbulent mixing and homogenization for cloud models applying more sophisticated representation of cloud microphysics. This aspect will be explored in future research.

Acknowledgments. This work was partially supported by the NOAA Grant NA05OAR4310107. Comments on the manuscript by Mirek Andrejczuk, Chris Jeffery, Steve Krueger, Szymon Malinowski, and Hugh Morrison are acknowledged. MMM's Bonnie Slagel provided editorial assistance. Computer time was provided by NSF MRI Grants CNS-0421498, CNS-0420873, and CNS-0420985; NSF sponsorship of the National Center for Atmospheric Research and the University of Colorado; and a grant from the IBM Shared University Research (SUR) program. Joanna Slawinska's assistance with BOMEX simulations is also acknowledged.

APPENDIX

Adiabatic Condensation Rate

For the adiabatic cloudy volume, the condensation rate can be derived from the rate of change of the saturated water vapor mixing ratio q_{ws} ; that is,

$$C^a = -\frac{dq_{ws}}{dt}, \quad (\text{A1})$$

where the superscript a refers to the adiabatic value of C . In the anelastic system, the saturated water vapor mixing ratio is given by (see discussion in section 7 and appendix A of Lipps and Hemler 1986)

$$q_{ws} = \frac{\varepsilon e_s}{p_e - e_s}, \quad (\text{A2})$$

where $\varepsilon = R_d/R_v$, R_d and R_v are the gas constants for dry air and water vapor, respectively; p_e is the environ-

mental pressure profile; and e_s is the saturated water vapor pressure, which is given by

$$e_s(T) = e_{00} \exp\left[\frac{L_v}{R_v} \left(\frac{1}{T_{00}} - \frac{1}{T}\right)\right], \quad (\text{A3})$$

where $T = \theta(p_e/p_{00})^{R_d/c_p}$, $p_{00} = 10^5$ Pa, and e_{00} and T_{00} are the reference values for the water vapor pressure and temperature, respectively. For the shallow warm convective clouds these can be selected as, say, $e_{00} = 1227$ Pa, and $T_{00} = 283.16$ K. Equation (A2) results in

$$\frac{dq_{ws}}{dt} = \frac{\partial q_{ws}}{\partial p_e} \frac{dp_e}{dt} + \frac{\partial q_{ws}}{\partial e_s} \frac{de_s}{dT} \frac{dT}{dt}. \quad (\text{A4})$$

Since $p_e = p_e(z)$ and it is hydrostatically balanced, it follows that $dp_e/dt = w dp_e/dz = -\rho_e g w$. Also, the Clausius–Clapeyron equation gives $de_s/dT = e_s L_v / R_v T^2$, and $dT/dt = L_v C^a / c_p - w g / c_p$. After inserting into (A4), applying (A1), and rearranging, the adiabatic condensate rate C^a is derived as

$$C^a = g w \frac{\rho_e q_{ws}}{p_e - e_s} \left(\frac{R_d L_v T_e}{R_v c_p T^2} - 1 \right) \times \left(1 + \frac{\rho_e q_{ws}}{p_e - e_s} \frac{R_d L_v^2 T_e}{R_v c_p T^2} \right)^{-1}. \quad (\text{A5})$$

For consistency, adiabatic condensate rate C^a has to be derived for each numerical model based on the specific set of model assumptions for the moist thermodynamics (i.e., the exact formulation of the saturated water vapor pressure e_s , and so forth).

REFERENCES

- Andrejczuk, M., W. W. Grabowski, S. P. Malinowski, and P. K. Smolarkiewicz, 2004: Numerical simulation of cloud–clear air interfacial mixing. *J. Atmos. Sci.*, **61**, 1726–1739.
- , —, —, and —, 2006: Numerical simulation of cloud–clear air interfacial mixing: Effects on cloud microphysics. *J. Atmos. Sci.*, **63**, 3204–3225.
- Austin, P. H., M. B. Baker, A. M. Blyth, and J. B. Jensen, 1985: Small-scale variability in warm continental cumulus clouds. *J. Atmos. Sci.*, **42**, 1123–1138.
- Bougeault, P., 1981: Modeling the trade-wind cumulus boundary layer. Part I: Testing the ensemble cloud relations against numerical data. *J. Atmos. Sci.*, **38**, 2414–2428.
- Brenguier, J.-L., and W. W. Grabowski, 1993: Cumulus entrainment and cloud droplet spectra: A numerical model within a two-dimensional dynamical framework. *J. Atmos. Sci.*, **50**, 120–136.
- Broadwell, J. E., and R. E. Breidenthal, 1982: A simple model of mixing and chemical reaction in turbulent shear layer. *J. Fluid Mech.*, **125**, 397–410.
- Grabowski, W. W., 1993: Cumulus entrainment, fine-scale mixing and buoyancy reversal. *Quart. J. Roy. Meteor. Soc.*, **119**, 935–956.

- , 1995: Entrainment and mixing in buoyancy reversing convection with applications to cloud-top entrainment instability. *Quart. J. Roy. Meteor. Soc.*, **121**, 231–253.
- , 2006: Indirect impact of atmospheric aerosols in idealized simulations of convective–radiative quasi equilibrium. *J. Climate*, **19**, 4664–4682.
- , and P. K. Smolarkiewicz, 1990: Monotone finite-difference approximations to the advection-condensation problem. *Mon. Wea. Rev.*, **118**, 2082–2097.
- , and T. L. Clark, 1991: Cloud–environment interface instability: Rising thermal calculations in two spatial dimensions. *J. Atmos. Sci.*, **48**, 527–546.
- , and —, 1993a: Cloud–environment interface instability. Part II: Extension to three spatial dimensions. *J. Atmos. Sci.*, **50**, 555–573.
- , and —, 1993b: Cloud–environment interface instability. Part III: Direct influence of environmental shear. *J. Atmos. Sci.*, **50**, 3821–3828.
- , and P. K. Smolarkiewicz, 1996: On two-time-level semi-Lagrangian modeling of precipitating clouds. *Mon. Wea. Rev.*, **124**, 487–497.
- Holland, J. Z., and E. M. Rasmusson, 1973: Measurements of the atmospheric mass, energy, and momentum budgets over a 500-kilometer square of tropical ocean. *Mon. Wea. Rev.*, **101**, 44–55.
- Jeffery, C. A., and J. M. Reisner, 2006: A study of cloud mixing and evolution using PDF methods. Part I: Cloud front propagation and evaporation. *J. Atmos. Sci.*, **63**, 2848–2864.
- Jensen, J. B., and M. B. Baker, 1989: A simple model for droplet spectral evolution during turbulent mixing. *J. Atmos. Sci.*, **46**, 2812–2829.
- Kerstein, A. R., 1988: A linear-eddy model of turbulent scalar transport and mixing. *Combust. Sci. Technol.*, **60**, 391–421.
- Klemp, J. B., and R. B. Wilhelmson, 1978: The simulation of three-dimensional convective storm dynamics. *J. Atmos. Sci.*, **35**, 1070–1096.
- Kogan, Y. L., and W. J. Martin, 1994: Parameterization of bulk condensation in numerical cloud models. *J. Atmos. Sci.*, **51**, 1728–1739.
- Krueger, S. K., 1993: Linear eddy modeling of entrainment and mixing in stratus clouds. *J. Atmos. Sci.*, **50**, 391–421.
- , C.-W. Su, and P. A. McMurtry, 1997: Modeling entrainment and finescale mixing in cumulus clouds. *J. Atmos. Sci.*, **54**, 2697–2712.
- Lewellen, W. S., and S. Yoh, 1993: Binormal model of ensemble partial cloudiness. *J. Atmos. Sci.*, **50**, 1228–1237.
- Lipps, F. B., and R. S. Hemler, 1986: Numerical simulation of deep tropical convection associated with large-scale convergence. *J. Atmos. Sci.*, **43**, 1796–1816.
- MacPherson, J. I., and G. A. Isaac, 1977: Turbulent characteristics of some Canadian cumulus clouds. *J. Appl. Meteor.*, **16**, 81–90.
- Malinowski, S. P., and I. Zawadzki, 1993: On the surface of clouds. *J. Atmos. Sci.*, **50**, 5–13.
- Margolin, L. G., P. K. Smolarkiewicz, and Z. Sorbjan, 1999: Large-eddy simulations of convective boundary layers using nonoscillatory differencing. *Physica D*, **133**, 390–397.
- Paluch, I. R., and D. G. Baumgardner, 1989: Entrainment and finescale mixing in a continental convective cloud. *J. Atmos. Sci.*, **46**, 261–278.
- Peters, N., 2000: *Turbulent Combustion*. Cambridge University Press, 304 pp.
- Radke, L. F., and P. V. Hobbs, 1991: Humidity and particle fields around some small cumulus clouds. *J. Atmos. Sci.*, **48**, 1190–1193.
- Siebert, H., K. Lehmann, and M. Wendisch, 2006: Observations of small-scale turbulence and energy dissipation rates in the cloudy boundary layer. *J. Atmos. Sci.*, **63**, 1451–1466.
- Siebesma, A. P., and Coauthors, 2003: A large eddy simulation intercomparison study of shallow cumulus convection. *J. Atmos. Sci.*, **60**, 1201–1219.
- Smolarkiewicz, P. K., and L. G. Margolin, 1997: On forward-in-time differencing for fluids: An Eulerian/semi-Lagrangian nonhydrostatic model for stratified flows. *Atmos.–Ocean*, **35**, 127–152.
- Sommeria, G., and J. W. Deardorff, 1977: Subgrid-scale condensation in models of non-precipitating clouds. *J. Atmos. Sci.*, **34**, 344–355.
- Su, C. W., S. K. Krueger, P. A. McMurtry, and P. H. Austin, 1998: Linear eddy modeling of droplet spectral evolution during entrainment and mixing in cumulus clouds. *Atmos. Res.*, **47–48**, 41–58.